

CHAPTER 140

INCIPIENT MOTION OF BREAKWATER ARMOR UNITS

J. A. Melby¹, M. ASCE, and N. Kobayashi², M. ASCE

ABSTRACT

This paper describes observations made of incipient motion on both stone and sphere armor layers. Velocity measurements were made during these experiments both inside and just outside the armor layer. It is shown that the vertical convective acceleration across the armor layer is proportional to the square of the vertical velocity. An incipient lifting motion criterion is derived based on Morison forcing for the dominant mode of motion: vertical lift under the steep breaking-wave face. The experimental observations and measurements are used to validate the incipient motion criterion for breakwater armor.

1 INTRODUCTION

Extensive research on breakwater armor stability has produced many empirical stability models. These models predict minor damage reasonably well. Many investigations have also quantified the wave forces on undamaged armor; and these force measurements have been used to compute more explicit stability criteria. But few studies have been done to observe and quantify the wave and structure conditions under which armor just begins to move, i.e. incipient armor motion.

The Iribarren (1938), Hudson (1958), and other empirical armor stability models are based on a free body analysis of an armor unit undergoing forcing due to breaking waves. Early stability models assumed the principle wave force was 1) due to down-or up-rush on an unsheltered and unrestrained unit, 2) drag dominance, and 3) that the drag force would be critical if the maximum horizontal fluid velocity was used, which was considered to be proportional to the incident wave celerity. But for an intact structure and prior to initiation of incipient motion, the armor units are typically partially hidden and restrained from up or down slope movement; so lift, inertia, and convection across the armor layer must be considered. Moreover, Sawaragi et. al. (1982) showed that the maximum fluid velocity on a rubble mound was not necessarily proportional to the wave celerity. Sigurdsson (1962) made force measurements on sphere armor at extremely steep slopes with an impermeable underlayer and with no underlayer and derived incipient equations of motion; but concluded by stating that the

¹ Res. Engineer, USAE Waterways Experiment Station, CERC, 3909 Halls Ferry Rd., Vicksburg, MS, 39180

² Professor, Center for Applied Coastal Research, University of Delaware, Newark, Delaware, 19716

dominant mechanism of initiation of armor motion was still unknown and required further investigation. Although many authors have discussed wave kinematics and dynamics on armor layers and the resulting forces, including Mizutani et. al (1992), Torum and van Gent (1992), Torum (1994), and Cornett and Mansard (1994), there have been few observations of incipient movement of armor units discussed in the literature. As such, the relationships between incipient motion, wave kinematics, and forces on armor units is still unknown.

Kobayashi et al. (1990) presented a numerical model for predicting the displacement of armor on a traditional rubble mound. The shallow water wave model interacted with a permeable flow model and hydrodynamic drag, inertia, and lift forces were computed using a Morison type of formulation (Morison et al. 1950). The model was limited to forces parallel to the structure because the hydrodynamics were one-dimensional vertically averaged. Torum and van Gent (1992) discussed a similar model and compared it to velocity measurements above a berm breakwater. Torum (1994) discussed the measurements further. Although two dimensional velocities were measured, vertical flow in the breaking wave was not modeled numerically. In addition, Torum noted that the inertial force was not well defined by the traditional inertia term of the Morison equation. Cornett and Mansard (1994) described an experiment where forces were measured on a panel of stones. This approach was unique and yielded insight into the average frictional force on sections of the armor layer. The results were used to develop a stability model for armor sliding.

The present article discusses a series of physical model experiments to identify and develop predictive models for breakwater armor incipient motion and to relate this motion to existing empirical stability relationships. The experiments were done in wave flumes at the Waterways Experiment Station in Vicksburg, Mississippi. The first experiment consisted of measuring wave-induced fluid velocities on and within the armor layer and runup/down. In addition, free surface oscillations were measured while observing armor motion on stone and Core-Loc armor. The observations from this early study led to an incipient motion experiment using a fixed-sphere armor layer with several loose spheres placed at various depths within the armor layer. A dominant incipient armor motion mode and predictive stability equation were verified.

EXPERIMENTAL SETUP

The initial experiments were conducted to determine the nature of armor incipient motion and surrounding flow. The instrumentation included a laser Doppler velocimeter (LDV), high resolution video, and runup and vertical free-surface-piercing gages near and within the armor layer. The experiments discussed herein were all carried out using regular monochromatic waves. The analysis techniques were done using short segments of between five and ten uniform waves to develop clear relationships between wave parameters and armor motion.

The primary study was done in a 46m long by 0.46m wide by 1m deep flume, with an offshore slope of 1V:30H. A conventional rubble mound cross section was constructed with various seaward slopes and armor types (Figure 1). Table 1 lists the different test plans. In this paper, only the sphere and stone armor plans will be discussed (Test Plans 3 and 4). Velocity measurements, sampled at 100 Hz, were made

throughout the water column from the toe to two armor dimensions above the still water level. The ranges of physical quantities and common dimensionless parameters for plans 3 and 4 are listed in Table 2.

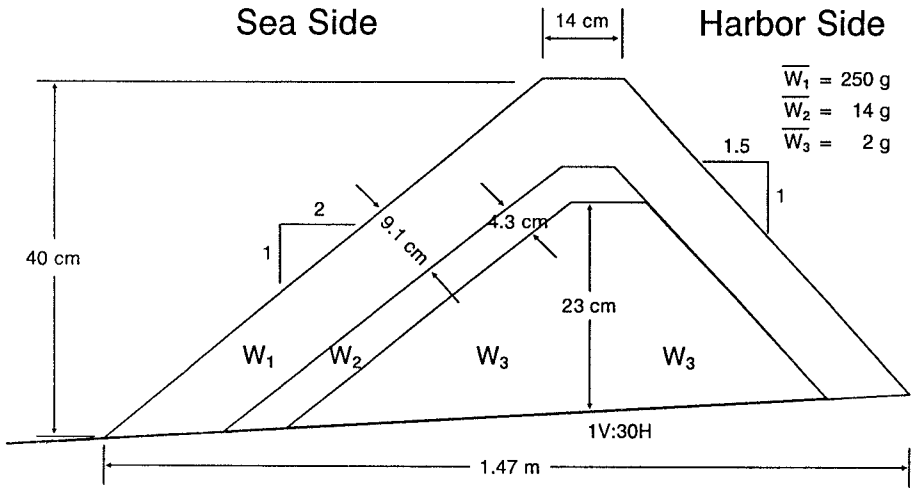


Figure 1. Definition sketch for typical structure profile.

Table 1. Experimental Plans							
Plan	Armor Type	Armor Weight W, g	Nominal Armor Dia. $D_n = (V)^{1/3}$ cm	Structure Slope, $\cot \theta$	Off-shore Slope $\cot \alpha$	Runup down Meas.	Force Meas.
1	Core-Loc	220	4.6	1.33	100	no	no
2	Core-Loc	105	3.6	1.5	20	no	no
3	Stone	200	4.6	2.0	30	yes	no
4	Sphere	58	3.8	2.0	30	yes	no
5	Sphere	212	5.6	2.0	30	yes	yes

Table 2. Ranges of Measured Physical Quantities and Common Dimensionless Parameters for Plans 3 and 4	
Parameter	Range
Wave height at toe, H_t	2.4 to 18 cm
Wave period, T	0.75 to 4.0 sec
Water depth at toe, d_t	15 to 24 cm
Wave steepness, $S_z = H_t / L_o$ L_o = deepwater wave length	0.007 to 0.1
Surf similarity parameter, $\xi = \tan \alpha / (H_t / L_o)^{1/2}$ $\tan \alpha = 1/30$ = beach slope	0.1 to 1.4
Surf similarity parameter, $\xi = \tan \theta / (H_t / L_o)^{1/2}$ $\tan \theta = 1/2$ = structure slope	1.5 to 21
Relative depth, d_t / L_o	0.009 to 0.28
Relative wave height, H_t / d_t	0.06 to 0.88

The LDV was a two-watt argon-ion two-component device assembled by the Dantec Corporation. The version used works in the back scatter mode using a non-intrusive probe which contains both the emission and receiving optics. The benefits of this device included nonintrusive measurements, small measurement volume, clean drop outs, high sampling rate, and no required calibration. The LDV is unique in that the probe can be pointed through the glass flume wall into the voids within the armor layer and allow measurements of the internal flow within the porous media. Many of the voids are more than a nominal armor diameter deep so the measurements can be made outside the flume wall boundary layer. One drawback to the LDV is it requires a full time operator with continuous attention to detail. Also, because of the small measurement volume, small changes in measurement location often yield large variations in measured velocities, especially near or within the breakwater armor layer. Therefore, the instrument requires many measurements to map the flow field. So data analysis requirements were substantial for this experiment.

The wave heights were determined using free surface measurements from a capacitance-type gage positioned at the location of the structure toe with no structure in place. Synthetic rubberized horse-hair mats were placed landward of the structure location to absorb the waves. The sampling rate for free surface measurements was 20 hz. The zero-downcrossing wave height was computed as the average height from a burst of approximately ten regular waves.

INCIPIENT MOTION OBSERVATIONS

Several dominant incipient motion modes were identified during the stone stability experiment in Plan 3, Table 1. The following descriptions pertain to initial armor

motion on an intact, as-built structure. Rolling was the only mode of motion for stones on the toe. Although both onshore and offshore motion was observed, the toe units always moved out of the layer in the onshore direction. For upslope armor, armor near the still water level was more likely to displace than armor in other areas. This appeared to be due to the fact that the armor was loosened in this area due to high velocities in the breaking wave jet. Once loosened, the motion would depend on the armor shape and its position. If the armor shape was flat, then the armor unit would flop back and forth until it rolled out of the armor layer, generally rolling upslope during uprush. If the armor shape was rounded, which was normally the case, the armor units would jump vertically under the steep wave face if the wave was severely plunging or collapsing. If the wave was surging, then loose units would only be displaced if they were exposed. There did not appear to be sufficient lift in downrush or uprush flows along the armor layer to displace the stones unless they were odd shaped (flat). The only displacement mechanism observed for rounded stones sufficiently hidden in the armor layer was uplift under the steep wave face.

These observations indicated that a fluid velocity or acceleration component in the vertical direction is normally required to initiate armor motion for hidden armor units. Additionally, this early qualitative study indicated that, for a wave of given energy, incipient motion was primarily influenced by wave shape, stone position, stone exposure, and stone looseness.

EXPERIMENTAL MEASUREMENTS

Throughout the experiments, vertical and horizontal wave velocities were measured in the vicinity of the armor layer. Figure 2 shows typical time series of the horizontal and vertical velocities on the structure. The sign convention was such that the horizontal velocity was positive seaward while the vertical velocity is positive upward. Note that the horizontal velocity amplitudes are very regular while the vertical velocity typically varies considerably. Figure 3 shows a velocity vector time series over one wave period, measured just above the armor layer one-third of the depth down from the still water level, and the wave profile at the point of maximum vertical velocity. The plot shows a large vertical velocity vector just below the steep wave front. Observed maximum stone movement for this wave profile position is also shown. Figure 4 shows an example of vertical velocities outside and inside the armor layer. The measurement locations for these time series are shown in Figure 5, where the structure slope is 1V:2H. Here it is clear that the velocities within the armor layer are highly irregular due to turbulence.

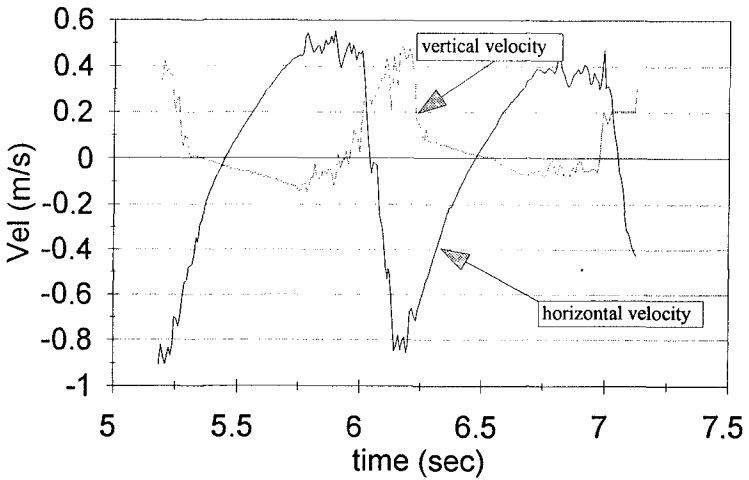


Figure 2. Velocity time series for one wave period, $H_t = 12\text{cm}$, $T = 1\text{ sec}$, $d_t = 24\text{ cm}$.

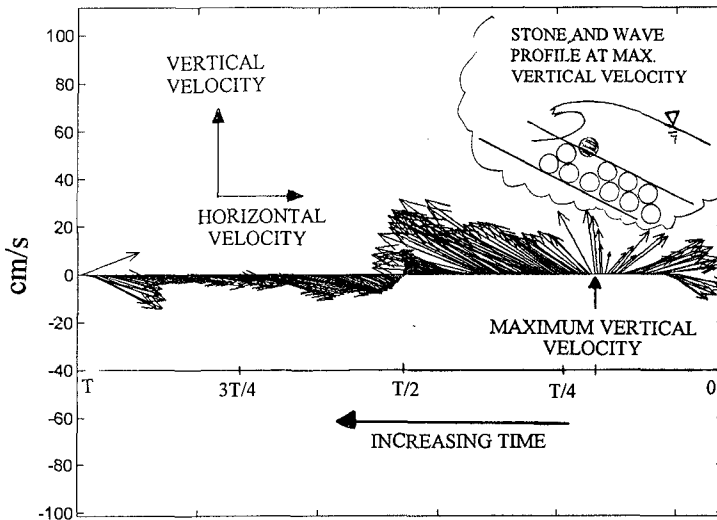


Figure 3. Velocity vector for one wave period for armor lifting.

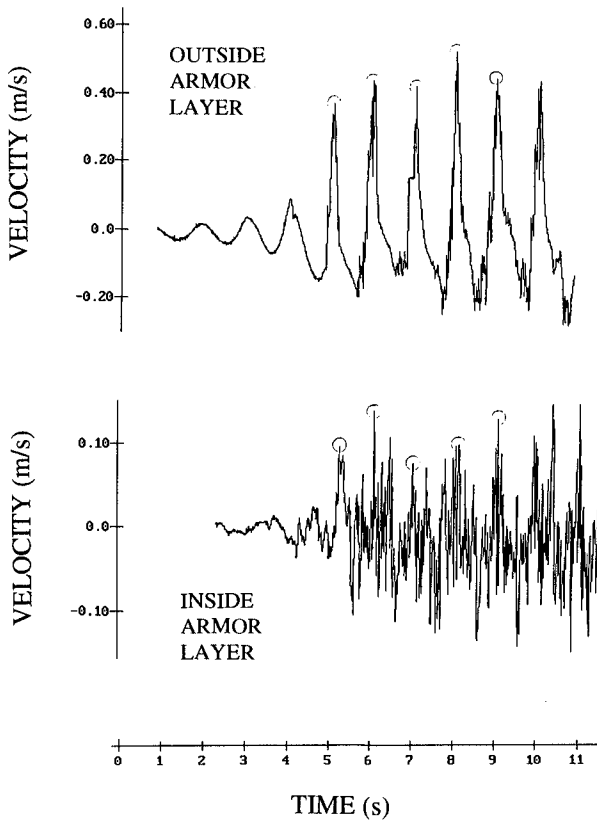


Figure 4. Vertical velocity time series outside and inside the armor layer

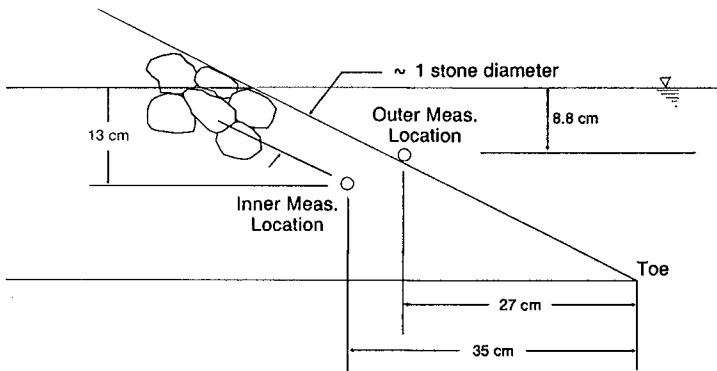


Figure 5. Measurement locations for vertical velocities shown in Figure 4.

Figure 6 shows a typical plot of vertical velocity $v_{1/3}/(gH_t)^{1/2}$, measured just above the armor layer at various depths, versus the square root of wave steepness, where $v_{1/3}$ is the average of the highest one-third peak velocities, g the gravitational acceleration, H_t the toe wave height, structure slope = 1V:2H, and L_o the deep water wave length. For simplicity, v is used instead of $v_{1/3}$ in Figure 6 and hereafter. Relative laser depth, rd , is the ratio of the depth of the laser to the depth at the toe, measured from the still water level. As noted by Sawaragi et al. (1982), maximum non-dimensional velocities commonly occurred for collapsing to plunging breaking waves. The peak vertical velocities for given wave period decreased downward with increase of rd in this figure.

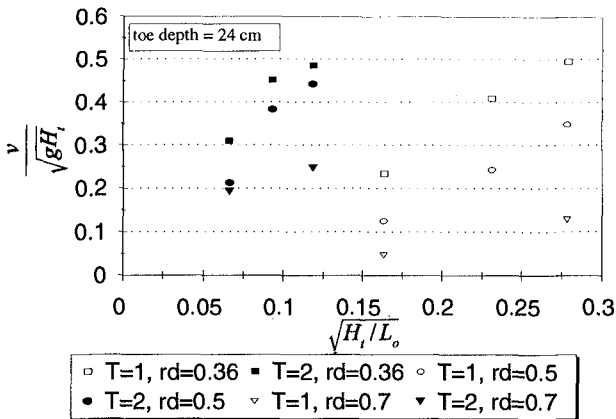


Figure 6. Maximum vertical velocity versus the square root of wave steepness for wave periods $T = 1$ and 2 s and relative depths $rd = 0.36, 0.5,$ and 0.7 .

INCIPIENT MOTION PREDICTION

The previous experimental results indicated that one of the dominant incipient motion modes was due to the vertical force occurring under the steep wave front. The balance of forces for vertical incipient armor motion with no external restraints yields the equality between the submerged armor weight and the vertical fluid force; $W' = F_v$. The vertical force at the steep wave front can be described by the Morison equation (Morison et al. 1950).

$$F_v = \frac{\rho}{2} A C_D v^2 + \rho V C_m \frac{dv}{dt} \quad (1)$$

where ρ = fluid density, A = cross sectional area of armor unit in direction of flow, C_D = drag coefficient, v = peak vertical velocity just above the armor layer as plotted in Figure 6, V = armor unit volume, C_m = inertia coefficient, and dv/dt = total fluid acceleration. The drag force can be expressed as a function of the armor nominal

diameter, D_n , by introducing an armor shape factor, K_A , as follows

$$A = K_A D_n^2 \tag{2}$$

The drag force in (1) is then given by

$$F_D = \rho D_n^2 C'_D v^2 ; \quad C'_D = \frac{K_A C_D}{2} \tag{3}$$

where the nominal diameter is defined as

$$D_n = V^{1/3} = \left(\frac{W}{\gamma_r} \right)^{1/3} \tag{4}$$

where W = armor weight, V = armor volume, and γ_r = armor specific weight.

At the point of maximum vertical fluid velocity, the local vertical fluid acceleration, $\partial v/\partial t$, and horizontal velocity, u , are negligible. As such, the total acceleration reduces to a convective term.

$$\left(\frac{dv}{dt} \right)_{\max} = \left(\frac{\partial v}{\partial t} + u \frac{\partial v}{\partial x} + v \frac{\partial v}{\partial y} \right)_{\max} \approx v \frac{\partial v}{\partial y} \tag{5}$$

where x = horizontal coordinate and y = vertical coordinate. If we assume the convective acceleration across the armor layer to vary linearly vertically, then the acceleration can be expressed as

$$\left(\frac{dv}{dt} \right)_{\max} \approx v \frac{\partial v}{\partial y} = K_c \frac{v^2}{D_n} \tag{6}$$

where K_c is an empirical coefficient on the order of unity. The maximum inertial fluid force in (1) can thus be reduced to

$$F_i = \rho D_n^2 C'_m v^2 \tag{7}$$

with

$$C'_m = K_c C_m \quad (8)$$

Substituting (3) and (7) into the stability criterion $W' = F_v$ with $W' = \rho g(S_r - 1)D_n^3$ yields a stability relation in form similar to Shields criterion for the initiation of motion of sediment particles

$$\frac{v_c^2}{D_n g(S_r - 1)} = (C'_D + C'_m)^{-1} \quad (9)$$

where S_r = armor specific gravity, g = acceleration of gravity, and v_c = critical vertical velocity at which armor just begins to lift. In terms of N_s = armor stability number, (9) becomes

$$N_s = \frac{H_c}{D_n(S_r - 1)} = \frac{gH_c}{v_c^2} (C'_D + C'_m)^{-1} \quad (10)$$

where H_c = critical wave height at toe. It is interesting to note that the stability number is primarily a function of the Froude number, $v_c / (gH_c)^{1/2}$. This formula ties the traditional stability relations to local vertical velocity measurements.

Based on results of detailed velocity measurements in the interior and just outside the armor layer, the vertical velocity gradient was found to be proportional to the ratio of the vertical velocity and the armor diameter, as assumed in (6). This is shown in Figure 7 for a typical case. The empirical convection coefficient is $K_c = 0.67$ for these tests.

The drag and inertia coefficients can be more accurately defined if we assume spherical armor. Based on previous studies of forces on armor by Mizutani et al. (1992) and Torum (1994), reasonable estimates for drag and inertia coefficients are $C_D = 0.8$ and $C_m = 0.4$ yielding

$$C'_D = \frac{K_A C_D}{2} \approx 0.5 \quad (K_A = 1.21) \quad (11)$$

$$C'_m = K_c C_m \approx 0.3 \quad (K_c = 0.67) \quad (12)$$

where $K_A = 1.21$ corresponds to a sphere. The critical vertical velocity, v_c , for the

incipient vertical armor movement reduces to

$$\frac{v_c^2}{D_n g(S_r - 1)} = 1.3 \tag{13}$$

where the critical vertical velocity, v_c , depends on the nominal diameter, D_n , and the specific gravity, S_r , only, for a loose armor unit.

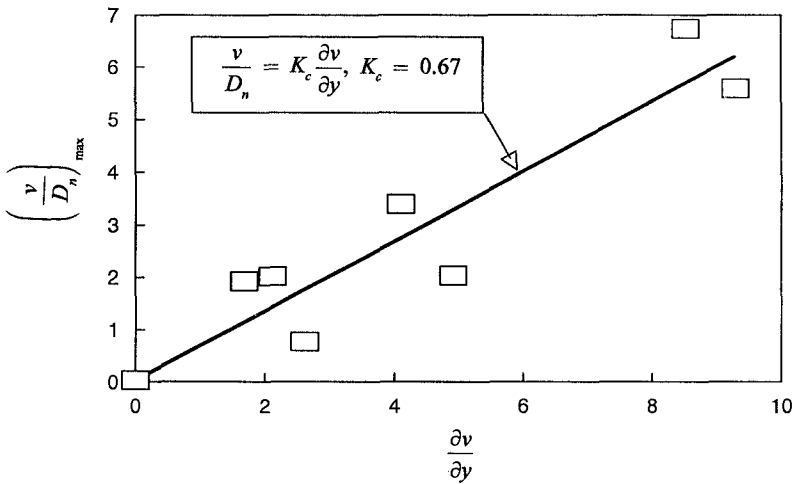


Figure 7. Vertical variation of vertical velocity under steep wave front.

Plan 4 in Table 1 was designed to test the above criterion. For Plan 4, the armor layer was constructed using silicon rubber spheres which were glued together and attached to an inflexible yet porous metal mat. The metal mat was placed directly on the underlayer and fixed to the flume walls. Several loose concrete spheres were placed in the armor layer along a line from above the still water level down to the toe. Each two loose spheres were separated by two glued spheres so that there was no interaction between loose spheres. The sphere layer of Plan 4 was constructed to have the minimum porosity of 0.33.

For Plan 4, the loose spheres would not move under any conditions unless they were slightly raised in the armor layer. This was accomplished by placing a 0.5-cm-thick washer under each sphere. The primary effect of this was to raise the porosity surrounding the loose sphere slightly, providing a path for water motion under the sphere. The only motion observed for the raised loose spheres was vertical motion under the steep wave front, following a slightly elliptical path, and landing back in their hole after the wave front passed. For tests with vertical velocities corresponding to the critical value, the spheres were just lifting off. For the larger vertical velocities, the

spheres were lifting entirely out of their initial holes, but settling back into their holes. Spheres at a depth of one-third the toe depth were the most mobile while spheres at the still water level were somewhat less mobile. This movement corresponded to the variation of the vertical velocities in the water column as shown in Figure 6. Figure 8 shows the incipient motion criterion versus wave steepness for Plan 4 using a few representative points from each motion category. The dark horizontal line represents the theoretical incipient motion criteria while the velocity measurements are represented by the dark dots. Observed movement is noted for each data point. For the drag and inertia coefficients selected, the incipient motion criteria agrees quite well with the observed movement.

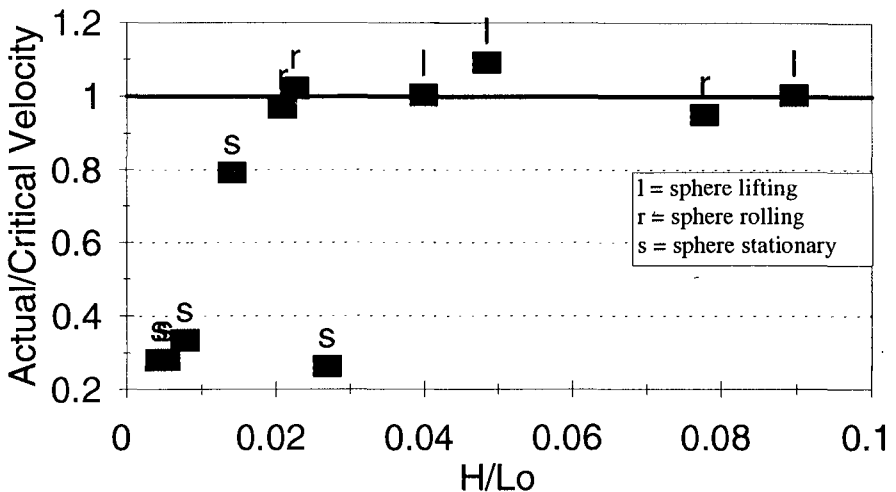


Figure 8. Incipient motion criterion versus wave steepness

CONCLUSIONS

Experiments on incipient motion of breakwater armor showed several modes of displacement. One dominant mode was due to vertical wave forces which are shown to occur at the point of maximum vertical velocity under the steep wave front. A simple relation was derived assuming a Morison-like wave force balanced by the armor unit submerged weight. The wave force model was composed of drag, due to the maximum vertical velocities, and inertia, due to the vertical convective accelerations. The maximum vertical convective acceleration is shown to be roughly linearly related to the square of the velocity, which puts the inertial force term into the same form as the drag term. The resulting incipient motion stability relation is similar in form to the Shields sediment motion criteria. Further, when expressed as a traditional stability number, incipient motion is shown to be a function of the Froude number, $v/(gH)^{1/2}$. The incipient motion criterion is shown to predict the incipient motion of spheres well for the conditions tested.

ACKNOWLEDGEMENT

This study was conducted and this article prepared with funding from the U.S. Army Engineer Coastal R&D Program. Permission to publish this article was granted by the Office, Chief of Engineers. Dr. Steven Hughes, U.S. Army Engineer Waterways Experiment Station, is acknowledged for his helpful suggestions regarding interpretation of data throughout the study.

REFERENCES

- Hudson, R.Y., 1958. "Design of quarry-stone a cover layers for rubble-mound breakaters," *RR 2-2*, USAE WES, Vicksburg, MS.
- Iribarren, R., 1938. "Una formula para el calculo de los diques en escoller (A formula for the calculation of rock-fill dikes)," *Revista de Obras Publicas*, Madrid, Spain. Translated by D. Heinrich, Tech. Rep. HE-116-295, Fluid Mech. Lab., Univ. of Calif., Berkeley, CA, 1948.
- Kobayashi, N, Wurjanto, A., and Cox, D. 1990. "Rock slopes under irregular wave attack," *Proc. 22nd ICCE*. ASCE, NY, NY, 1306-1319.
- Mizutani, N., Iwata, K., Rufin, T.M., and Kurata, K. 1992. "Laboratory investigation of the stability of a spherical armor unit of a submerged breakwater," *Proc. 23rd ICCE*. ASCE, NY, NY, 1400-1413.
- Morison, J., O'Brien, M., Johnson, J., Scaaf, S. 1950. "The force exerted by surface waves on piles," *Petroleum Trans.* 189, TP 149-154.
- Sawaragi, T., Iwata, K., and Kobayashi, N., 1982. "Conditions and probability of occurrence of resonance on steep slopes of coastal structures," *Coastal Engineering in Japan*, 25, 75-90.
- Sigurdsson, G. 1962. "Wave forces on breakwater capstones," *J. Wirwy. and Harb. Div.*, ASCE, WW3, 27-60.
- Torum, A., van Gent, M. 1992. "Water particle velocities on a berm breakwater," *Proc. 23rd ICCE*, ASCE, NY, NY, 1651-1665.
- Torum, A. 1994. "Wave-induced forces on armor units on berm breakwaters," *J. Wirway, Port, Coast., and Oc. Engrg.*, ASCE, 120(3), 251-268.